Comparative Study on Oil-Based and Water-Based Hybrid Nanofluids with Stagnation-Point Flow Due to Variable Viscosity and Thermal Conductivity

***Dr Radhika M**

Department of Mathematics, G.F.G.C., Kolar, Karnataka, India

***Corresponding Author**

DOI: https://doi.org/10.51584/IJRIAS.2026.11100026

Received: 15 October 2026; Accepted: 20 October 2026; Published: 02 November 2026

ABSTRACT

Researchers recently developed hybrid nanofluids to address drawbacks of existing nanofluids, including clogging, low stability, high pressure drop, and expensive production. Here, viscosity and thermal conductivity vary with temperature, and by considering these variations, we can predict the flow behaviour. We consider the stretching sheet with an external magnetic field to conduct the flow. We convert the flow equations of momentum and heat transfer, which prevail in the present problem with boundary conditions, into nonlinear coupled ordinary differential equations using relevant similarity transformations.

Graphs illustrate and analyse how the non-dimensional parameter influences the velocity and temperature profiles. We compared the heat transfer rate for various values of the Prandtl number under some special assumptions with published research works and obtained satisfactory results in alignment with the papers. The results show that the heat transfer rate is sufficiently large for MWCNT-Alumina/engine oil hybrid nanofluid compared to MWCNT-Alumina/water hybrid nanofluid. Because of this, engineers and industry professionals can use MWCNT-Alumina/engine oil hybrid nanofluid as an efficient coolant.

Keywords: Variable viscosity, variable thermal conductivity, hybrid nanofluid velocity ratio parameter. 2010 Mathematics Subject Classification: 80A20

INTRODUCTION

The new heat transfer coolant, nanofluid, was discovered through recent research in nanotechnology. Nanofluid [1], pioneered by Choi, is a new type of fluid that disperses oxide ceramics (Al_2O_3, CuO), metal c arbides (Sic, nitrides AlN, SiN), metal (Al, Cu), non-metals (graphite, carbon nanotubes) liquidly. By adding nanoparticles, heat transfer and fluid flow can be altered, and thermal properties and stability can be improved. It has many applications in the cooling of microchips, medical applications, space and defence, nuclear system cooling, industrial cooling, solar water heating, refrigeration, thermal storage, biomedical applications, transportation, power generation, aerospace, chemical engineering, manufacturing, and electronic applications. But nanofluids exhibit some drawbacks, such as clogging and reduced stability. The specific heat capacity of nanofluid is lower than that of base fluids. Nanofluids are not used commonly in the industry because of their higher production cost. To overcome these drawbacks of nanofluids, many researchers started using hybrid nanofluids by mixing two or more dissimilar nanoparticles that have different physical and chemical properties in the base fluid. It attributes a good aspect ratio, higher heat transfer rate, better thermal network. The main purpose of using mixed nanofluids is to obtain the correct properties of each nanoparticle. Some nanoparticles may have good thermal properties, or some may have good rheological properties. By using hybrid nanofluids, one can combine all excellent features of each nanoparticle that are required for many practical applications. CNTs have very high electrical and thermal conductivity, mechanical resistance, chemical stability, and physical strength. These properties of CNTs have attracted many researchers to develop hybrid nanofluids consisting of CNTs with metallic or nonmetallic nanoparticles. Hybrid nanofluids consisting of CNTs are used in electrochemical sensors,

biosensors, and nanocatalysts. Engine oil is used for both cooling and lubrication in internal combustion engines. The friction between moving parts of the engine will be decreased, and the generated heat will be transferred by the use of engine oil. This results in an improvement in the heat transfer rate, and ultimately the efficiency and lifespan of the engine will become better. In this study, we compare the heat transfer rate of both MWCNT-Alumina/water and MWCNT-Alumina/engine oil hybrid nanofluids.

Mohammed A et al. [2] investigated the effect of convective hybrid CNT- Al_2O_3 nanofluid. He got the result that heat transfer increases with the increasing value of the Rayleigh number. Mohsen Izadi [3] discussed natural convection of MgO/Ag –water hybrid nanofluid flow because of the impact of the variable magnetic field in a porous medium including the heater. The temperature gradient close to the heater increases with increasing values of the porosity coefficient. Tanzila Hayat et al. [4] analysed three-dimensional rotation of Ag-CuO/water nanofluid because of the impact of heat generation, chemical reaction and thermal radiation. They found that hybridity enhances the heat transfer rate. The Heat transfer rates of Cu-water nanofluid flow and Cu-Al2O3/water hybrid nanofluid flow across a stretched sheet were compared by Suriya Uma Devi et al. [5]. Based on their findings, they concluded that hybrid nanofluid has a higher heat transfer rate than nanofluid and is more effective in cooling processes. Sandesh et al.'s [6] investigation of hybrid nanofluids' thermal conductivity took into account the impact of nanoparticle size and surface area.

The thermal conductivity of CNT-water and CNT-Al2O3/water hybrid nanofluids was experimentally studied by Mageshbabu et al. [7]. They concluded that the hybrid nanofluid had a higher specific heat capacity and thermal conductivity than the CNT-water nanofluid. According to the findings of their experiment, Ester et al. [8] conducted an investigation on the heat-conducting properties of CNT-Al2O3/water combined nanofluids and the impact of temperature and concentration. They discovered that the solid volume percentage of the nanoparticles influences the thermal conductivity of the nanofluid. Sheren A. Kaska et al. [9] carried out a CFD analysis to predict the heat transfer and pressure drop inside a horizontal flat-tube by considering AlN- Al_2O_3 /water hybrid nanofluid. They reported that with the rising values of Reynolds number and volume fraction of nanoparticles, pressure drop increases. Mehdi Bahiraei et al[10] evaluated the thermohydraulic properties of graphene silver nanoparticles hybrid nanofluid in a microchannel heat sink. They found that with increasing value of concentration or Reynolds number of nanoparticles enhances cooling efficiency. Fitnat Saba et al. [11] employed a study on heat transfer of Cu-Al_2O_3 –hybrid nanofluid inside a rectangular channel. They found that platelet-shaped nanoparticles displayed a better heat transfer rate than the cylinder- and brick-shaped nanoparticles. Experimental research on the thermal conductivity of hybrid nanofluid CuO/MWCNT-water was conducted by Masond Zadlehast et al. [12]. They demonstrated how thermal conductivity increased with increasing volume fraction and temperature. The point at which the fluid flow's local velocity becomes zero is known as the stagnation point.

Stagnation point flow happens when the fluid flow approaches any solid surface, and it divides into opposite directions along the surface. It has many applications, such as in groundwater flows, extrusion of a polymer sheet from a die, petroleum industries, cooling of electronic devices by fans, cooling of nuclear reactors during emergency shutdown and hydrodynamic processes. A computational investigation of the effect of the magnetic field in a porous medium on the stagnation point flow of both Al_2O_3-water nanofluid and CuO-water nanofluid was proposed by Mabood et al. [13]. He discovered that the skin friction coefficient is increased by the porosity. The MHD stagnation point flow of CuO-water and Ag-water nanofluids across a moving plate was examined by Fazle Mabood et al. [14]. They came to the conclusion that when the magnetic field increases, the local Nusselt number gets stronger. The stagnation point flow of two nanofluids comprising single- and multiwalled carbon nanotubes was compared by Noreen et al. They concluded that the local Nusselt number rises with enhancing values of thermal conductivity parameter, slip parameter, radiation parameter, and convective parameter. Mohammad Youseti et al. [16] analytically presented a model of steady stagnation point flow of TiO2-CuO/water hybrid nanofluid past a circular cylinder. They demonstrated that the temperature distribution and heat transfer rate improve with hybridity. Ghadikolaei et al. [17] analysed the effect of the magnetic field by considering the stagnation flow of a hybrid nanofluid. They considered a TiO2–Cu/water hybrid nanofluid over a stretching sheet. They used the RKF method to solve non-linear differential equations. They concluded that hybrid nanofluids are more

ISSN No. 2454-6194 | DOI: 10.51584/IJRIAS |Volume XI Issue X October 2026

effective than nanofluids, and platelet-shaped nanoparticles are more effective than brick- and cylindrically shaped nanoparticles.

In the above-discussed papers, viscosity and the thermal conductivity were considered as constants. But in the actual behaviour of the flow, viscosity and thermal conductivity won't stay as invariants. Studies that consider variable viscosity and thermal conductivity have many applications in the underground storage system and the extraction of geothermal energy. Eiyad Ab Nada [18] presented a mathematical model of CuO-water nanofluid flow because of variable thermal conductivity and viscosity in horizontal annuli. He found that for Reynolds numbers greater than or equal to $10^{4,}$ the average Nusselt number decreased with the rising value of the volume fraction of nanoparticles. Manjunatha et al[19] explored the heat transfer of dusty fluid with the combined impact of variable viscosity and the thermal conductivity over an unsteady stretching sheet. They got the result that the fluid that has low thermal conductivity can be considered for effective cooling.

The three-dimensional stagnation point flow of Cu-water and Cu- Al_2O_3hybrid nanofluids through a circular cylinder was covered by Nadeem et al. [20]. It is reported that the hybrid nanofluid has a higher heat transfer rate than the nanofluid. Cu- Al_2O_3/water hybrid nanofluid flow across a stretching sheet was taken into consideration by Manjunatha et al. [21] in order to forecast the combined influence of free convection and changing viscosity.

They found that the temperature of Cu- Al_2O_3/water hybrid nanofluid increases with the increasing value of the variable viscosity parameter.

As far as the authors are aware, no research has been done to compare the heat transfer of hybrid nanofluids, such as MWCNT- Al_2O_3/water and MWCNT- Al_2O_3/engine oil, with stagnation point flow and the combined effects of thermal conductivity and variable viscosity. We examined the effects on the temperature and velocity profiles of the two hybrid nanofluids with variable viscosity parameter B, variable thermal conductivity parameter S, magnetic field parameter M, and velocity ratio parameter.

Model Of The Problem

Analysis is done on the two-dimensional hybrid nanofluid boundary layer flow together with a stretching sheet that has a stagnation point. We allowed viscosity and the thermal conductivity to vary with the temperature. We treated the motion of the sheet along the x-axis, and the y-axis is taken normal to it. Along the y-direction, a uniform magnetic field B is applied. A hybrid nanofluid is obtained by mixing MWCNT-Al_2O_3 into water and also into engine oil. Spherical-shaped nanoparticles are taken into consideration.

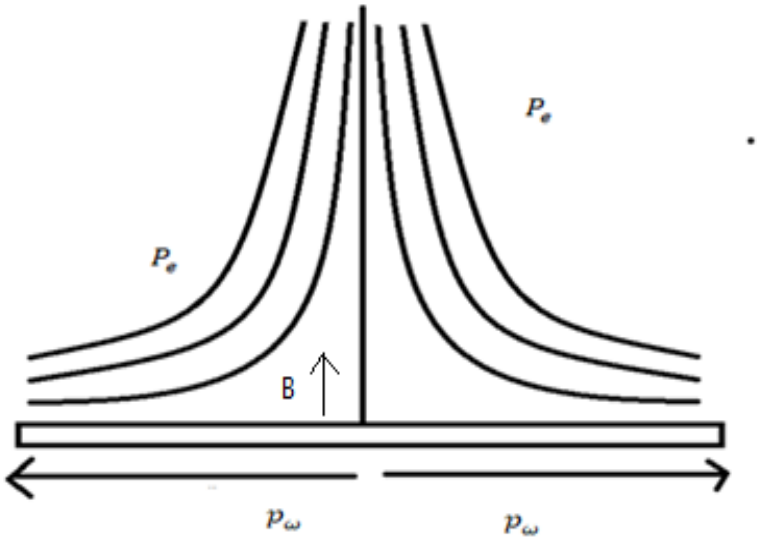


Figure 1:Physical drawing of the problem.

ISSN No. 2454-6194 | DOI: 10.51584/IJRIAS |Volume XI Issue X October 2026

Governing equations that are prevalent to the present problem, as per the above assumptions, are given by

$$\frac{\partial \mathrm{p}}{\partial \mathrm{x}} + \frac{\partial \mathrm{q}}{\partial \mathrm{y}} = 0 \quad (1)$$

$$\left(\mathrm{p}\frac{\partial \mathrm{p}}{\partial x} + \mathrm{q}\frac{\partial \mathrm{p}}{\partial y}\right) = \frac{1}{\rho_{\mathrm{hnf}}}\ \frac{\partial}{\partial \mathrm{y}}\left(\mu_{hnf}\frac{\partial \mathrm{p}}{\partial \mathrm{y}}\right) + P_e\frac{\partial P_e}{\partial \mathrm{x}} + \frac{\sigma {B_1}^2}{\rho_{\mathrm{hnf}}}(P_e - p) \quad (2)$$

$$\left(\mathrm{p}\frac{\partial \mathrm{T}}{\partial x} + \mathrm{q}\frac{\partial \mathrm{T}}{\partial y}\right) = \frac{1}{(\rho c_{\mathrm{p})\mathrm{hnf}}}\ \frac{\partial}{\partial \mathrm{y}}\left(K_{hnf}\frac{\partial \mathrm{T}}{\partial \mathrm{y}}\right) \quad (3)$$

Viscosity and thermal conductivity are varied according to

$$\mu_{f=}\mu_{0\,e^{-B\theta}}(\eta),\ K_f = K_\infty(1+S\theta),\ \theta = \frac{T-T_\infty}{T_\omega - T_\infty} \quad (4)$$

The boundary conditions in the current problem are

$$\mathrm{p}=p_\omega,\quad \mathrm{q}=0,\quad \mathrm{T}=T_\omega \quad \text{at } y=0$$

$$p \to P_e,\quad T \to T_\infty \quad \text{as } y \to \infty \quad (5)$$

	$\boldsymbol{\rho}$(Kgm$^{-3)}$	c_p(JKg^{-1}K^{-1})	k(Wm^{-1}K^{-1})
Water	997.1	4179	0.613
Engine oil	920	1670	0.138
MWCNT	1600	796	3000
Al_2O_3	3970	765	40

Table 1. Thermophysical properties of base fluids: water and engine oil, and nanoparticles MWCNT and alumina Al_2O_3

Properties	**Hybrid Nanofluid**
Density$(kg\ m^{-3})$	$\rho_{hnf} = \left[(1-\emptyset_2)\{(1-\emptyset_1)\rho_f + \emptyset_1\rho_{s1}\} + \emptyset_2\rho_{s2}\right]$
Heat Capacity (JK^{-1})	$(\rho Cp)_{hnf} = \left[(1-\emptyset_2)\{(1-\emptyset_1)(\rho Cp)_f + \emptyset_1(\rho Cp)_{s1}\} + \emptyset_2(\rho Cp)_{s2}\right]$
Viscosity $(Ns.m^{-2})$	$\mu_{hnf} = \frac{\mu_f}{(1-\emptyset_1)^{2.5}(1-\emptyset_2)^{2.5}}$
Thermal Conductivity $(W.K^{-1}.m^{-1})$	$\frac{K_{hnf}}{K_{bf}} = \frac{K_{s2}+(n-1)K_{bf}-(n-1)\phi_2(K_{bf}-K_{s2})}{K_{s2}+(n-1)K_{bf}+\phi_2(K_{bf}-K_{s2})}$ Where $\frac{K_{bf}}{K_f} = \frac{K_{s1}+(n-1)K_f-(n-1)\phi_1(K_f-K_{s1})}{K_{s1}+(n-1)K_f+\phi_1(K_f-K_{s1})}$

Table 2: Thermophysical Model

ISSN No. 2454-6194 | DOI: 10.51584/IJRIAS |Volume XI Issue X October 2026

Also, n = 3 is for spherical nanoparticles.

We consider the following set of similarity variables involving the dimensionless variable η as

$$p = a\,x\,f'(\eta)\ , q = -\sqrt{a\,\vartheta_f}\,f(\eta)\ ,\ \eta = \sqrt{\frac{a}{\vartheta_f}}\ y, \theta = \frac{T-T_\infty}{T_\omega - T_\infty} \qquad (6)$$

where η is the transformed one-dimensional axis. Equation (1) is automatically satisfied. Equations (2) and (3) convert into the following ordinary differential equations:

$$f''' - B\theta' f'' = (1-\varphi_1)^{2.5}(1-\varphi_2)^{2.5}\left\{M\ f' - M\,\varepsilon + \left[(1-\emptyset_2)\left\{(1-\emptyset_1) + \emptyset_1\frac{\rho_{s1}}{\rho_f}\right\} + \emptyset_2\frac{\rho_{s2}}{\rho_f}\right]((f')^2 - ff'' - \varepsilon^2)\right\} \qquad (7)$$

$$(1+S\theta)\theta'' + S(\theta')^2 =$$

$$\left(\frac{K_f}{K_{hnf}}\right)\left(\frac{(\rho c_p)_{hnf}}{(\rho c_p)_f}\right)\left[(1-\emptyset_2)\left\{(1-\emptyset_1) + \emptyset_1\frac{(\rho Cp)_{s1}}{(\rho Cp)_f}\right\} + \emptyset_2\frac{(\rho Cp)_{s2}}{(\rho Cp)_f}\right]P_r(2\theta f' - f\theta') \qquad (8)$$

Boundary conditions (5) and (6) are transformed into

$$f'(0) = 1,\quad f(0)=0\ ,\quad \theta(0) = 1,\ f'(\infty) \to \varepsilon\ ,\quad \theta(\infty) \to 0. \qquad (9)$$

The local skin friction coefficients and the local Nusselt number can be expressed as

$$Re_x = \frac{x p_\omega,}{\nu_f}\quad , Cf_x = \frac{\mu_{hnf}}{\rho_f\, p_{\omega,^2}}\left(\frac{\partial p}{\partial y}\right)_{y=0}, Nu_x = \left(\frac{-K_{hnf}}{K_f}\right)\frac{x\left(\frac{\partial T}{\partial y}\right)_{y=0}}{(T_\omega - T_\infty)}$$

$$Re_x^{\frac{1}{2}} Cf_x = \frac{f''(0)}{(1-\varphi_1)^{2.5}(1-\varphi_2)^{2.5}}\quad , Re_x^{\frac{-1}{2}} Nu_x = \left(\frac{-K_{hnf}}{K_f}\right)\theta'(0) \qquad (10)$$

METHODOLOGY

The coupled nonlinear ordinary differential equations (7) and (8) with boundary equations (9) are solved numerically using MATLAB bvp4c algorithm. For numerical results, we kept the following values as common throughout the study, except for the varied values shown in graphs and tables.$\varphi_1 = 0.1,\ \varphi_2 = 0.005,\ M = 1,\ \in = 0.5\ S = 0.1,$ and B=1. We considered MWCNT- Al_2O_3–water hybrid nanofluid and MWCNT- Al_2O_3–engine oil hybrid nanofluid. Table 3 exhibits the comparison of values of $-\theta'(0)$ for various values of Prandtl number. We got a satisfactory result with published papers of [26],[27],[28],[29] and [30].

$\mathbf{P_r}$	Grubka &Bobba[26]	Sharena et al. [27]	Noorzehan et al [28]	Gireesha et al. [29]	Sandeep et al. [30]	Present study
1	1.3333	1.3333	1.3333	1.3333	1.3333	1.33333086579675
3	2.5097	2.5097	2.5097	-	-	2.50971545474265
10	4.7969	4.7969	4.7969	4.7968	4.7968	4.79680688408748

Table 3. Comparison of $-\theta'(0)$ for various values of P_r.

ISSN No. 2454-6194 | DOI: 10.51584/IJRIAS |Volume XI Issue X October 2026

RESULTS AND DISCUSSION

Data in Tables 4 and 5 display numeric values of the local skin friction coefficients $Re_x^{\frac{1}{2}}Cf_x$ for different amounts of modifiable thermal conductivity factor S and local skin friction coefficients $Re_x^{\frac{1}{2}}Cf_x$ and local Nusselt number $\frac{-k_{hnf}}{k_f}\theta'(0)$ for various values of v variable viscosity parameter B. Table 4 illustrates that the rise in S decreases the local Nusselt number of both hybrid nanofluids. Table 5 shows that the rise in B decreases both the local skin friction coefficient and the local Nusselt number of both hybrid nanofluids. Table 6 exhibits variation of $f''(0)$ and $-\theta'(0)$ for various values of B, M and $\in$ of MWCNT- Al_2O_3 /water MWCNT- Al_2O_3/engine oil hybrid nanofluids. Table 6 reveals that the increasing values of B and M decrease f'’0 and the heat transfer rate $-\theta'(0)$ of both hybrid nanofluids. But $f''(0)$ and heat transfer rate $-\theta'(0)$ of both hybrid nanofluids increase with the rising value of both $\in$.

Figure. 2 and 3 are plotted to illustrate the consequence of the non-dimensional similarity variable η and non-dimensional velocity component $f'(\eta)$ for both MWCNT-Alumina/water and MWCNT-Alumina/engine oil hybrid nanofluids for various values of the variable viscosity parameter B. Figure 2 shows that velocity profile $f'(\eta)$ decreases with increasing value of B for the MWCNT-Alumina/water hybrid nanofluid. In Figure. 3 also the same trend is exhibited for the velocity profile of MWCNT-Alumina/engine oil hybrid nanofluid. Figure. 4,5 reveal the variation of the variable viscosity parameter B on the temperature profiles of both MWCNT-Alumina/water and MWCNT-Alumina/engine oil hybrid nanofluid. From Figures 4 and 5, we can observe that the temperature field increases with the rising values of B. The Physical reason behind this fact is the increasing value of the viscosity parameter enhances the resistance to the flow, which results in the decline of the velocity boundary layer thickness and results in a flattening of the velocity profile. But rising values of B tend to enhance the thermal boundary layer thickness, and it gives rise to the magnification of the temperature profile.

Figure 6 and Figure 7 exhibit the relation between similarity variable η and nondimensional velocity component $f'(\eta) of$ both MWCNT-Alumina/water and MWCNT-Alumina/engine oil hybrid nanofluids for various values of the magnetic field parameter M. From Figure. 6 and 7, we can understand that the velocity field decrease with M. But in Figures 8 and 9 we can visualise that the temperature profile increases with M.This is because the magnetic field parameter develops a Lorentz force, which acts opposite to the fluid flow and it declines the velocity boundary layer and thermal boundary layer thickness.

Figures 10,11,12 and 13 are sketched to discuss the variation of the velocity profiles and the temperature profiles of both MWCNT-Alumina/water and MWCNT-Alumina/engine oil hybrid nanofluid for various values of the velocity ratio parameter $\in$.

Figures 10 and 11 show that an increase in the velocity ratio parameter $\in$ enhances velocity profile $f'(\eta)$ for both hybrid nanofluids. But Figures 12 and 13 illustrate that the temperature profile diminishes with increasing values of the velocity ratio parameter $\in$. When $\in$>0, near to the stagnation point the straining motion is enhanced, and it leads to the augmentation of acceleration of the external stream. This is because the increase in the velocity ratio parameter increases the velocity boundary layer but decreases the thermal boundary layer.

Figure. 14and 15 reveal the variation of variable thermal conductivity parameter S on the temperature profile of both MWCNT-Alumina/water and MWCNT-Alumina/engine oil hybrid nanofluid. Figures 14 and 15 describe that the rise in the variation of thermal conductivity parameter increases temperature profile $\theta(\eta)$. Physically, it means that increasing the value of S increases the thermal boundary layer thickness. This is the reason for the enhancement of the temperature field.

The local skin friction coefficient and the local Nusselt number are visualised through Figures 14 and 15 for the variation of the velocity ratio parameter $\in$. With increasing values of $\in$, the local Nusselt number increases, but the local skin friction coefficient decline.

ISSN No. 2454-6194 | DOI: 10.51584/IJRIAS |Volume XI Issue X October 2026

CONCLUSION

We conducted a numerical analysis to examine the impact of temperature-dependent viscosity and thermal conductivity on the fluid flow and heat transfer in stagnation point flow using MWCNT-Alumina/water and MWCNT-Alumina/engine oil. The governing equations that occur in the present problem are reformed into nonlinear coupled ordinary differential equations. Using the inbuilt function bvp4c in MATLAB, these equations are solved. The velocity profile and the temperature profile of both hybrid nanofluids are portrayed for various values of non-dimensional parameters through graphs and discussed. Based on the graphs and tables, we concluded that.

- The increasing values of $\in$ intensifying the velocity profile of both hybrid nanofluids
- The rise in $\in$ decreases the temperature profile of both hybrid nanofluids.
- The temperature profile of both hybrid nanofluids enhances with the rising values osS.
- The increasing value of B intensifies the temperature profile but deprive the velocity profile of both hybrid nanofluids.
- As the variable thermal conductivity parameter increases, the local Nusselt number decreases.
- Local skin friction coefficient and local Nusselt number are both decreased by increasing values of the variable viscosity parameter.
- When compared to MWCNT-Alumina/water hybrid nanofluid, the heat transfer rate between MWCNT-Alumina and engine oil is suitably high. Due to this MWCNT-Alumina/engine oil hybrid nanofluid is an efficient coolant for engineering and industrial applications.
- We compared the heat transfer rate $-\theta'(0)$ for distinct values of Prandtl number Pr and assent with the available works of literature.

REFERENCES

1. S.U.S. Choi, Enhancing thermal conductivity of fluids with nanoparticles, International Mechanical Engineering Congress and Exposition, San Francisco, vol. 66, USA, ASME, FED 231/MD, 1995, pp. 99–105.
2. Mohammed A. Tashkandia and Abdelkarim Aydi, Heat Transfer Intensification In A 3d Cavity Using Hybrid CNT- Al_2O_3 (15-85%) Nanofluid**,** Frontiers in Heat and Mass Transfer (FHMT), 11, 27 (2018).
3. Mohsen Izadi, Nemat M. Maleki, Ioan Pop,and S.A.M. Mehryan, (2019) "Natural convection of a hybrid nanofluid subjected to the non-uniform magnetic field within porous medium including circular heater", International Journal of Numerical Methodsfor Heat & Fluid Flow.
4. Tanzila Hayat and S. Nadeem, Heat transfer enhancement with Ag–CuO/water hybrid nanofluid, Results in Physics 7 (2017) 2317–2324.
5. Suriya Uma Devi. S. and S. P. Anjali Devi, Heat Transfer Enhancement Of $Cu - Al_2O_3$ /Waterhybrid Nanofluid Flow Over A Stretching Sheet, Journal Of The Vol. 36, Issue 2, Pp. 419-433, 2017, Nigerian Mathematical Society
6. Sandesh S. Chougule and Santosh Kumar Sahu, Model of Heat Conduction in Hybrid Nanofluid, 2013 IEEE International Conference on Emerging Trends in Computing, Communication and Nanotechnology
7. Mageshbabu Devarajan, Nagarajan Parasumanna Krishnamurthy, Madhu Balasubramanian, Bharathwaj Ramani, Somchai Wongwises3, Kabeel Abd El-Naby4, and Ravishankar Sathyamurthy, Thermophysical properties of CNT and CNT/ Al_2O_3 hybrid nanofluid, Micro & Nano Letters.

8. Mohammad Hemmat Esfe, Seyfolah Saedodin, Wei-Mon Yan, Masoud Afrand1, Nima Sina, Study on thermal conductivity of water-based nanofluids with hybrid suspensions of CNTs/ Al_2O_3 nanoparticles, J Therm Anal Calorim (2016) 124:455–460.
9. Sheren A. Kaskaa, Rafeq A. Khalefa, and Adnan M. Hussein, Hybrid nanofluid to enhance heat transfer under turbulent flow in a flat tube, Case Studies in Thermal Engineering 13 (2019) 100398.
10. Mehdi Bahiraei, Mohammad Jamshidmofid, Marjan Goodarzi, Efficacy of a hybrid nanofluid in a new microchannel heat sink equipped with both secondary channels and ribs, Journal of Molecular Liquids
11. Fitnat Saba, Naveed Ahmed, Umar Khan, Asif Waheed, Muhammad Rafiq and Syed Tauseef Mohyud-Din, Thermophysical Analysis of water Based (Cu– Al_2O_3)Hybrid Nanofluid in an Asymmetric Channel with Dilating/Squeezing Walls Considering Different Shapes of Nanoparticles, Applied sciences, 2018, 8, 1549.
12. Masoud Zadkhast, Davood Toghraie, and Arash Karimipour, Developing a new correlation to estimate the thermal conductivity of MWCNT-CuO/water hybrid nanofluid via an experimental investigation, J Therm Anal Calorim (2017) 129:859–867
13. F. Mabood, S. Shateyi, M.M. Rashidi, E. Momoniat, and N. Freidoonimehr, MHD stagnation point flow heat and mass transfer of nanofluids in a porous medium with radiation, viscous dissipation, and chemical reaction, Advanced Powder Technology 27 (2016) 742–749
14. Fazle Mabood, Nopparat Pochai, Stanford Shateyi, Stagnation Point Flow of Nanofluid over a Moving Plate with Convective Boundary Condition and Magnetohydrodynamics, Journal of Engineering, Volume 2016, Article ID 5874864.
15. Noreen Sher Akbar, and Zafar Hayat Khan, Effect of variable thermal conductivity and thermal radiation with CNTS suspended nanofluid over a stretching sheet with convective slip boundary conditions: Numerical study, Journal of Molecular Liquids 222 (2016) 279–286
16. Mohammad Yousefi, Saeed Dinarvand, Mohammad Eftekhari Yazdi, and Ioan Pop, (2018), Stagnation point flow of an aqueous titania-copper hybrid nanofluid toward a wavy cylinder, International Journal of Numerical Methods for Heat & Fluid Flow, Vol. 28 Issue: 7, pp.1716-1735.
17. S.S. Ghadikolaei, M. Yassari, H. Sadeghi, Kh. Hosseinzadeh, and D.D. Ganji, Investigation on thermophysical properties of Tio2–Cu/H2O hybrid nanofluid transport dependent on shape factor in MHD stagnation point flow, Powder Technology 322 (2017) 428–438.
18. Eiyad Abu-Nada, Effects of Variable Viscosity and Thermal Conductivity of CuO-Water Nanofluid on Heat Transfer Enhancement in Natural Convection: Journal of Heat Transfer MAY 2010, Vol. 132 / 052401-7
19. S. Manjunatha a, and B.J. Gireesha, Effects of variable viscosity and thermal conductivity on MHD flow and heat transfer of a dusty fluid, Ain Shams Engineering Journal (2016) 7, 505–510.
20. S.Nadeem ,NadeemAbbas, and A.U.Khan, Characteristics of three-dimensional stagnation point flow of a Hybrid nanofluid past a circular cylinder, Results in Physics, Volume 8, March 2018, Pages 829-835.
21. S. Manjunatha, B. Ammani Kuttan, S. Jayanthy, B. J. Gireesha, and M. Archana, Heat transfer enhancement in the boundary layer flow of hybrid nanofluids due to variable viscosity and natural convection, April 2019, Heliyon 5(4):e01469
22. A. A. Minea and M. G. Moldoveanu**,** Overview of Hybrid Nanofluids Development and Benefits, Journal of Engineering Thermophysics,2018, vol 27, No 4, pp 507-514.
23. Gabriela Huminic, and Angel Huminic, Hybrid nanofluids for heat transfer applications – A state-of-the-art review, International Journal of Heat and Mass Transfer 125 (2018) 82–103.
24. Huminic, G., and Huminic, A. (2018). Hybrid nanofluids for heat transfer applications – A state-of-the-art review, International Journal of Heat and Mass Transfer, 125, 82–103.
25. Rakesh K. Bumataria , N.K. Chavda, and Hitesh Panchal, Current research aspects in mono and hybrid nanofluid based heat pipe technologies, Heliyon 5 (2019) e01627.
26. Grubka L.J, and Bobba K .M 1985, Heat transfer characteristics of a continuous stretching surface

with variable temperature, Journal of Heat transfer, 107,250-284
27. Sharena M I, Anati A, and Sharidan S,2016, Magnetohydrodynamic flow of dusty fluid past a vertical stretching sheet with hall effect, Seminar Kebangsan Sains Mathematik 23,24-26, November 2015, AIP conference proceedings, 1750,020005.
28. Noorzehan Fazahiyah Md Shab, and Anati Ali, Hydromagnetic boundary layer flow of a dusty fluid in a porous medium over a stretching sheet with slip effect, Malaysian Journal of Fundamental and Applied Sciences, vol 13, No 3(2017)170-173.
29. B.J. Gireesha, G K Ramesh, H.J. Lokesb, and C.S. Bagewadi, Boundary Layer Flow and Heat Transfer of a Dusty Fluid over a Stretching Vertical Surface, Applied Mathematics, 2011, 2, 475-481
30. Sandeep Naramgari, C. Sulochana, and Banglore Rushi KUMAR, Flow and Heat Transfer in MHD Dusty Nanofluid Past a Stretching/ Shrinking Surface with Non-Uniform Heat Source/Sink, Walailak Journal of Science and Technology (WJST) Vol 14, No 2 (2017)

s	$\frac{-\mathbf{k_{hnf}}}{\mathbf{k_f}}\boldsymbol{\theta'(0)}$	
	MWCNT-Alumina/water	**MWCNT-Alumina/engine oil**
1	2.631479869	17.08531374
2	2.052170279	13.39893671
3	1.729704867	11.34298735

Table 4. Numerical values of Local Nusselt number $\frac{-k_{hnf}}{k_f}\theta'(0)$.

B	$Re_x^{\frac{1}{2}}Cf_x$		$\frac{-\mathbf{k_{hnf}}}{\mathbf{k_f}}\boldsymbol{\theta'(0)}$	
	MWCNT-Alumina/water	**MWCNT-Alumina/engine oil**	**MWCNT-Alumina/water**	**MWCNT-Alumina/engine oil**
1	-1.62833376	-2.35955036	3.88203767	25.0395323
2	-2.570711047	-5.40809409	3.78229942	24.6508158
3	-3.778264046	-11.3463101	3.67429012	24.0080917

Table 5. Numerical values of the local skin friction coefficients $Re_x^{\frac{1}{2}}Cf_x$ and local Nusselt number $\frac{-k_{hnf}}{k_f}\theta'(0)$.

B	**M**	$\in$	$\boldsymbol{f''(0)}$		**-θ '(0)**	
			MWCNT-Alumina/water	**MWCNT-Alumina/engine oil**	**MWCNT-Alumina/water**	**MWCNT-Alumina/engine oil**
1	1	0.5	-1.23574249063057	-2.86732458414572	2.87069264996196	18.503940496397 6
2	1	0.5	-1.95091261366450	-4.10420260844935	2.79693811752391	18.216683274357 5
3	1	0.5	-2.86732458414572	-8.61071476786497	2.71706730755268	17.741717163642 1

1	**2**	0.5	-1.23574249063057	-2.03512416672169	2.84866276858164	17.672438913521 8
1	**3**	0.5	-1.49165962380215	-2.24445041316266	2.83058656874803	17.612128721553 3
1	1	**0.6**	-1.01806348089327	-1.47181320805681	2.91508585166416	18.571225176796 3
1	1	**0.7**	-0.785039906399713	-1.13248945180032	2.95941447587330	18.640012396642 8

Table 6. Variation of $f''(0)\ and\ \theta'(0)$ for various values $\varphi_2, B, M, and\ \in$ of MWCNT- Al_2O_3/water hybrid nanofluid and MWCNT- Al_2O_3/engine oil hybrid nanofluid

Nomenclatures

$p(m.s^{-1})$	Velocity component along the x-axis
$q(m.s^{-1})$	Velocity component along the y-axis
$p_w = ax(m.s^{-1})$	The stretching velocity of the sheet
$p_e = cx(m.s^{-1})$	The ambient fluid velocity
$T(K)$	The temperature of the hybrid nanofluid
$T_w(K)$	Temperature distribution in the stretching surface.
$T_\infty(K)$	Temperatures far off from the wall.
$\mu_{hnf}(Ns.m^{-2})$	Effective viscosity of the hybrid nanofluid
$\mu_f(Ns.m^{-2})$	Effective viscosity of the base fluid
$\mu_0(Ns.m^{-2})$	Reference viscosity of the fluid.
$v_f(kg.m^{-1}s^{-1})$	- Dynamic viscosity of the base fluid.
$\rho_{hnf}\ (kg\ m^{-3})$	The density of the hybrid nanofluid
$\rho_f(kg\ m^{-3})$	The density of the base fluid.
$\rho_{s1}(kg.m^{-3})$	The density of nanoparticles MWCNT
$\rho_{s2}(kg.m^{-3})$	The density of nanoparticles Al_2O_3
ϕ_1	The volume fraction of nanoparticles Multiwalled carbon nanotube MWCNT.
ϕ_2	The volume fraction of nanoparticles Al_2O_3
$K_f\ (W.K^{-1}.m^{-1})$	Thermal conductivity of the base fluid
$K_{hnf}\ (W.K^{-1}.m^{-1})$	Thermal conductivity of the hybrid nanofluid
$K_{s1}\ (W.K^{-1}.m^{-1})$	Thermal conductivity of nanoparticles Multiwalled carbon nanotube MWCNT.
$K_{s2}\ (W.K^{-1}.m^{-1})$	Thermal conductivity of nanoparticles Al_2O_3
$K_{bf}\ (W.K^{-1}.m^{-1})$	Thermal conductivity of the base fluid
$K_\infty\ (W.K^{-1}.m^{-1})$	Ambient thermal conductivity of the base fluid
B	Variable viscosity parameter.
S	Variable thermal conductivity parameter.

$\varepsilon = \frac{c}{a}$	Velocity ratio parameter
c, a	Constants
$(\rho c_p)_f$ (J/K/m3)	Volumetric heat capacities of the base fluid.
$(\rho c_p)_{hnf}$ (J/K/m3)	Volumetric heat capacities of the hybrid nanofluid.
$(\rho c_p)_{s1}$ (J/K/m3)	Volumetric heat capacities of the nanoparticles MWCNT
$(\rho c_p)_{s2}$ (J/K/m3)	Volumetric heat capacities of the nanoparticles Al_2O_3
$Re_x = \frac{xp}{\upsilon_f}$	Local Reynolds number.
Nu_x	Local Nusselt number.
Cf_x	Local skin friction coefficient.
$P_r = \frac{(\mu c_p)_f}{k_f}$	Prandtl number.
K $(kg.ms^{-2})$	-Stokes resistance.
B_1 (tesla)	-Magnetic field flux density.
$\boldsymbol{\sigma}$ (Siemens per meter)	-Electrical conductivity
$M = \frac{\sigma {B_1}^2}{a\rho_f}$	-Magnetic field parameter.

Figures

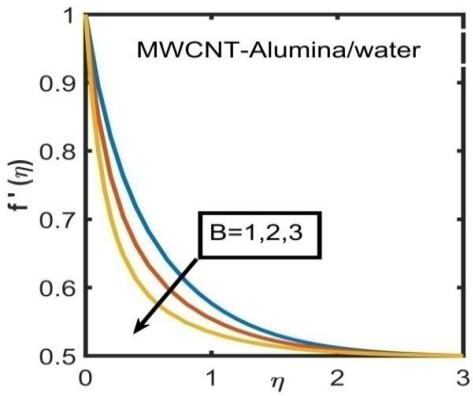


Figure 2.Velocity profile for various values of B

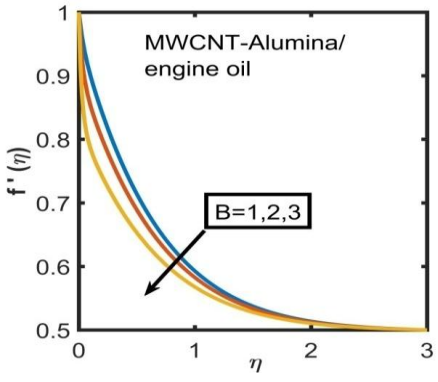


Figure 3.Velocity profile for various values of B

ISSN No. 2454-6194 | DOI: 10.51584/IJRIAS |Volume XI Issue X October 2026

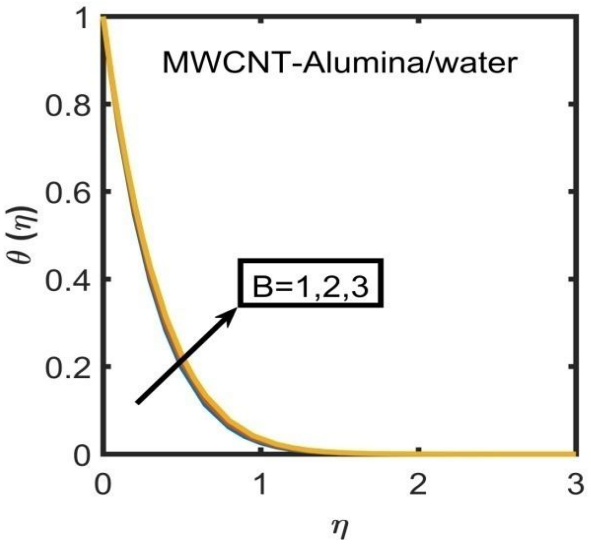


Figure 4.Temperature profile for various values of B

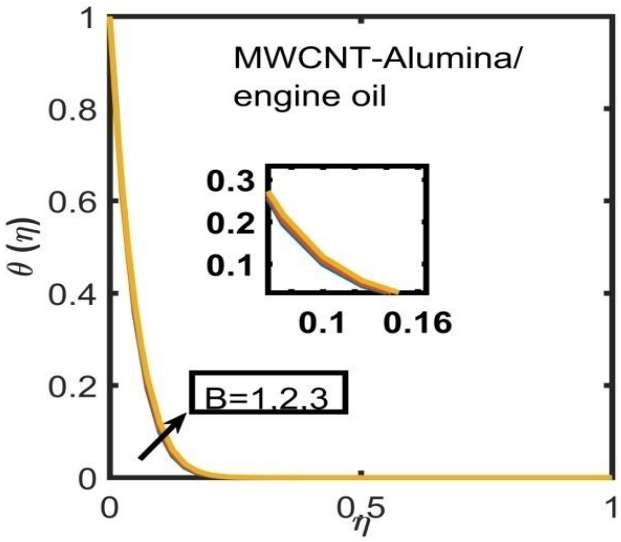


Figure 5.Temperature profile for various values of B

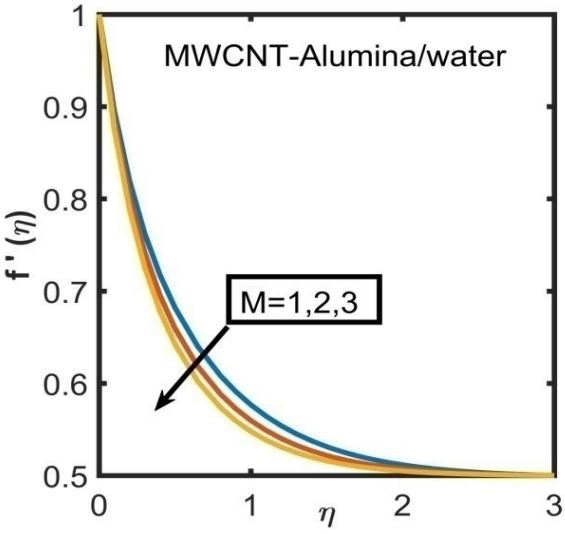


Figure 6.Velocity profile for various values of M.

ISSN No. 2454-6194 | DOI: 10.51584/IJRIAS |Volume XI Issue X October 2026

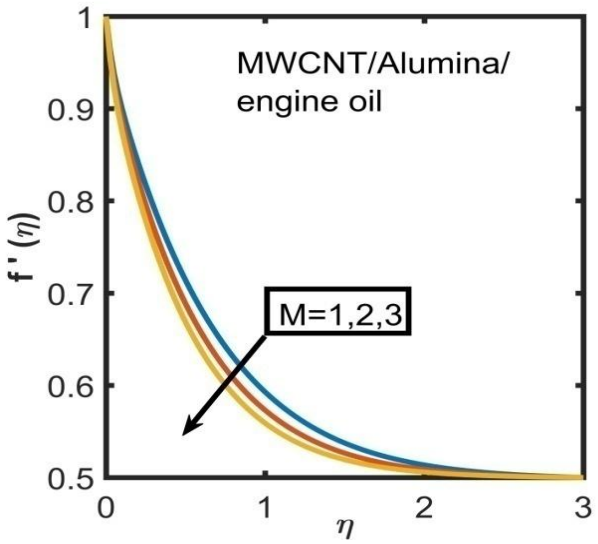


Figure 7.Velocity profile for various values of M.

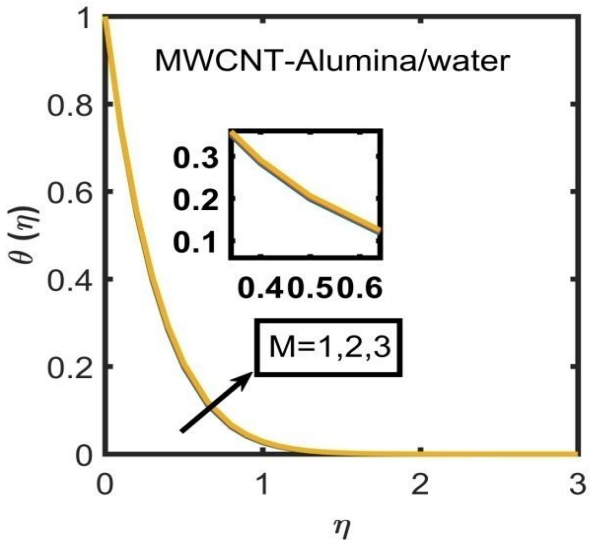


Figure 8.Temperature profile for various values of M

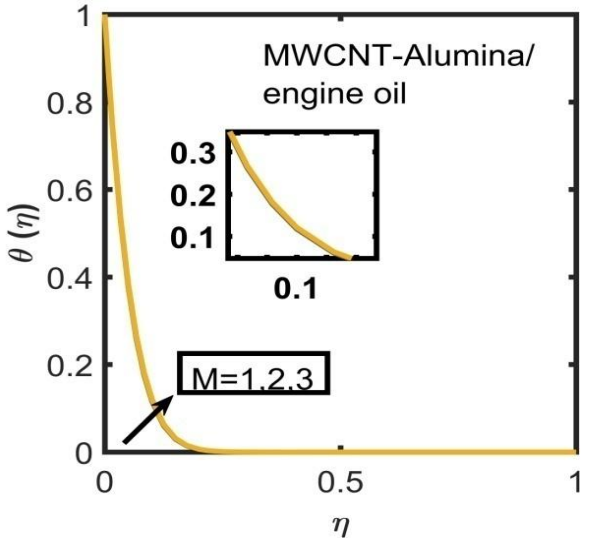


Figure 9 Temperature profile for various values of M

ISSN No. 2454-6194 | DOI: 10.51584/IJRIAS |Volume XI Issue X October 2026

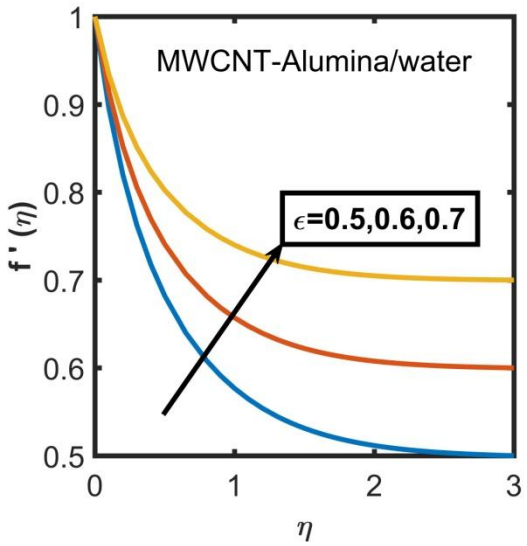


Figure 10.Velocity profile for various values of ∈.

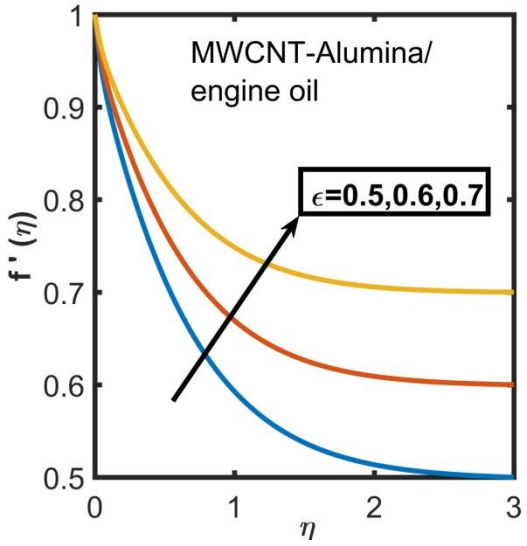


Figure 11.Velocity profile for various values of ∈ .

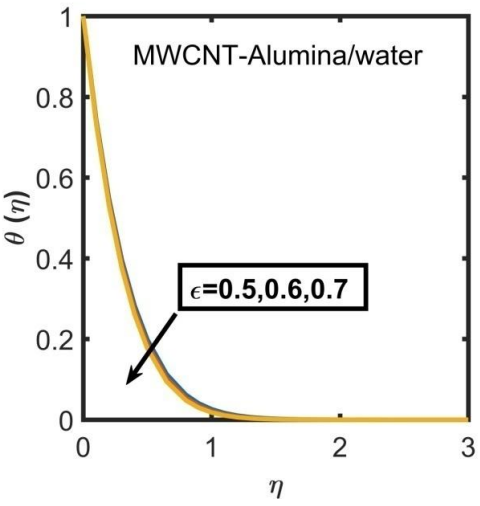


Figure 12.Temperature profile for various values of ∈.

ISSN No. 2454-6194 | DOI: 10.51584/IJRIAS |Volume XI Issue X October 2026

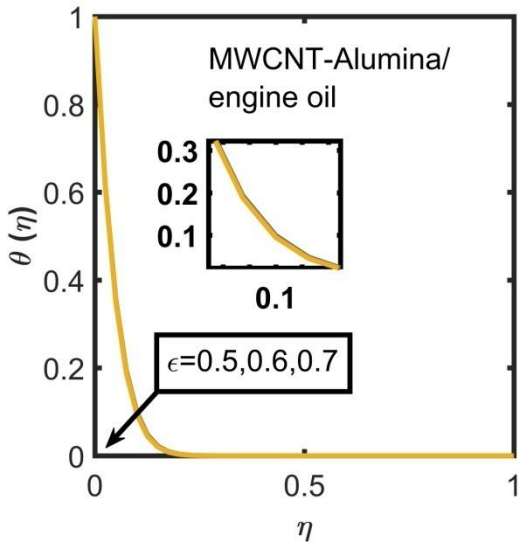


Figure 13.Temperature profile for various values of ∈

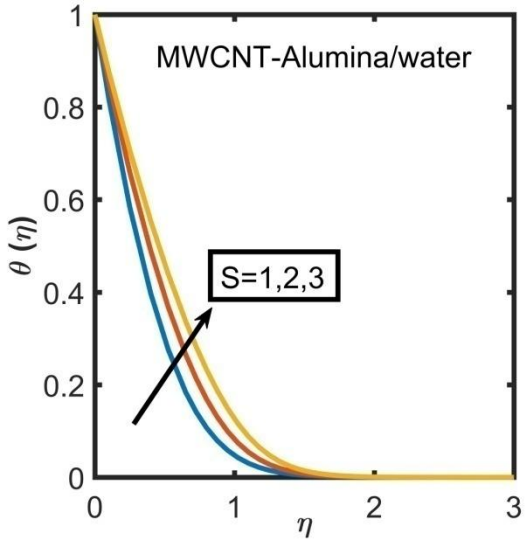


Figure 14.Temperature profile for various values of S.

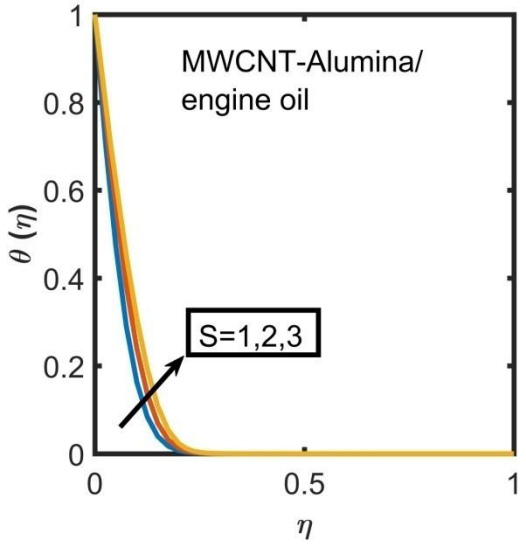


Figure 15.Temperature profile for various values of S.

ISSN No. 2454-6194 | DOI: 10.51584/IJRIAS |Volume XI Issue X October 2026

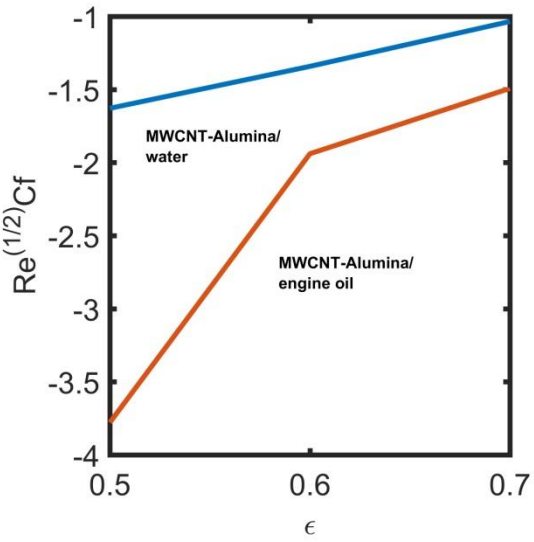


Figure 16.The local skin friction coefficient for various values of ∈.

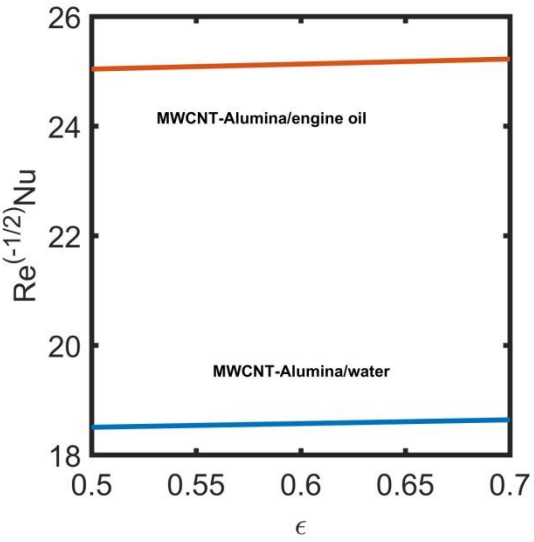


Figure 17.The local Nusselt number for various values of ∈